

# 1 Atmospheric $\Delta^{17}\text{O}(\text{NO}_3^-)$ reveals nocturnal chemistry dominates nitrate production 2 in Beijing haze

3 Pengzhen He<sup>1</sup>, Zhouqing Xie<sup>1,2,3\*</sup>, Xiyuan Chi<sup>1</sup>, Xiawei Yu<sup>1</sup>, Shidong Fan<sup>1</sup>, Hui Kang<sup>1</sup>, Cheng Liu<sup>1,2,3</sup>, Haicong Zhan<sup>1</sup>

4 <sup>1</sup>Anhui Province Key Laboratory of Polar Environment and Global Change, School of Earth and Space Sciences, University  
5 of Science and Technology of China, Hefei, Anhui 230026, China.

6 <sup>2</sup>Center for Excellence in Urban Atmospheric Environment, Institute of Urban Environment, Chinese Academy of Sciences,  
7 Xiamen, Fujian 361021, China.

8 <sup>3</sup>Key Lab of Environmental Optics and Technology, Anhui Institute of Optics and Fine Mechanics, Chinese Academy of  
9 Sciences, Hefei, Anhui 230031, China.

10

11 \*Corresponding to: Zhouqing Xie ([zqxie@ustc.edu.cn](mailto:zqxie@ustc.edu.cn))

12

13 **Abstract.** The rapid mass increase of atmospheric nitrate is a critical driving force for the occurrence of fine-particle  
14 pollution (referred to as haze hereafter) in Beijing. However, the exact mechanisms for this rapid increase of nitrate mass has  
15 been not well constrained from field observations. Here we present the first observations of the oxygen-17 excess of  
16 atmospheric nitrate ( $\Delta^{17}\text{O}(\text{NO}_3^-)$ ) collected in Beijing haze to reveal the relative importance of different nitrate formation  
17 pathways, and we also present the simultaneously observed  $\delta^{15}\text{N}(\text{NO}_3^-)$ . During our sampling period, 12h-averaged mass  
18 concentrations of  $\text{PM}_{2.5}$  varied from 16 to 323  $\mu\text{g m}^{-3}$  with a mean of  $(141 \pm 88 \text{ (1SD)}) \mu\text{g m}^{-3}$ , with nitrate ranging from 0.3  
19 to 106.7  $\mu\text{g m}^{-3}$ . The observed  $\Delta^{17}\text{O}(\text{NO}_3^-)$  ranged from 27.5 ‰ to 33.9 ‰ with a mean of  $(30.6 \pm 1.8) \text{‰}$  while  $\delta^{15}\text{N}(\text{NO}_3^-)$   
20 ranged from  $-2.5 \text{‰}$  to 19.2 ‰ with a mean of  $(7.4 \pm 6.8) \text{‰}$ .  $\Delta^{17}\text{O}(\text{NO}_3^-)$ -constrained calculations suggest nocturnal  
21 pathways ( $\text{N}_2\text{O}_5 + \text{H}_2\text{O}/\text{Cl}^-$  and  $\text{NO}_3 + \text{HC}$ ) dominated nitrate production during polluted days ( $\text{PM}_{2.5} \geq 75 \mu\text{g m}^{-3}$ ) with the  
22 mean possible fraction of 56 – 97 %. Our results illustrate the potentiality of  $\Delta^{17}\text{O}$  in tracing nitrate formation pathways,  
23 future modelling work with the constraint of isotope data reported here may further improve our understanding of nitrogen  
24 cycle during haze.

## 25 1 Introduction

26 Severe and frequent haze pollution has become a crucial threat for the air quality in megacity Beijing and the North  
27 China Plain in recent years. The high concentrations of  $\text{PM}_{2.5}$  (particulate matter with an aerodynamic diameter equal or  
28 less than 2.5  $\mu\text{m}$ ) during severe haze, of which the hourly average can reach 1000  $\mu\text{g m}^{-3}$  (Zheng et al., 2015a), is harmful

29 to the public health by contributing to cardiovascular morbidity and mortality (Cheng et al., 2013; Brook et al., 2010).  
30 Nitrate is an important component of PM<sub>2.5</sub>, accounting for 1–45 % of PM<sub>2.5</sub> mass in Beijing and North China Plain (Wen et  
31 al., 2015; Zheng et al., 2015a; Zheng et al., 2015b). The main formation pathways of atmospheric nitrate in urban area are  
32 summarized in Fig. 1, which includes: (i) NO<sub>2</sub> oxidation by OH radical in the gas-phase, (ii) heterogeneous uptake of NO<sub>2</sub> on  
33 wet aerosols, (iii) NO<sub>3</sub> radical reacting with hydrocarbon (HC), and (iv) heterogeneous uptake of N<sub>2</sub>O<sub>5</sub> on wet aerosols and  
34 chlorine-containing aerosols. Since OH radical is mainly present in the daytime while NO<sub>3</sub> radical and N<sub>2</sub>O<sub>5</sub> are mainly  
35 present in the nocturnal atmosphere (Brown and Stutz, 2012), NO<sub>2</sub> + OH is usually referred as the daytime nitrate formation  
36 pathway while N<sub>2</sub>O<sub>5</sub> + H<sub>2</sub>O/Cl<sup>-</sup> and NO<sub>3</sub> + HC are referred as nocturnal formation pathways (Vicars et al., 2013; Sofen et al.,  
37 2014). During haze in Beijing, the mixing ratio of daytime OH is modelled to be low (Zheng et al., 2015b; Rao et al., 2016)  
38 while relatively high mixing ratio of nocturnal N<sub>2</sub>O<sub>5</sub> is observed in several studies (Wang et al., 2017a; Li et al., 2018; Wang  
39 et al., 2017b), therefore, nocturnal pathways are suggested to be most responsible for the high concentrations of atmospheric  
40 nitrate during haze (Su et al., 2017; Pathak et al., 2009; Pathak et al., 2011). In addition, the high PM<sub>2.5</sub> concentration and  
41 relative humidity during haze in Beijing favors heterogeneous reactions, which renders NO<sub>2</sub> + H<sub>2</sub>O being a potentially  
42 significant pathway for nitrate production (Wang et al., 2017d; Tong et al., 2015; Zheng et al., 2015a).

43 Nitrogen isotopic composition of nitrate ( $\delta^{15}\text{N}(\text{NO}_3^-)$ , wherein  $\delta^{15}\text{N} = (R_{\text{sample}}/R_{\text{reference}} - 1)$  with  $R$  representing isotope  
44 ratios of  $^{15}\text{N}/^{14}\text{N}$  in the sample and the reference atmospheric N<sub>2</sub>) is useful in tracing source of its precursor NO<sub>x</sub> (Xiao et al.,  
45 2015; Beyn et al., 2014; Fang et al., 2011; Hastings et al., 2013). Anthropogenic sources of NO<sub>x</sub> such as coal combustion are  
46 generally enriched in  $\delta^{15}\text{N}$  while natural NO<sub>x</sub> sources such as soil emissions or lightning typically have negative or zero  $\delta^{15}\text{N}$   
47 signature (Hoering, 1957; Yu and Elliott, 2017; Felix et al., 2012). Therefore highly positive values of observed  $\delta^{15}\text{N}(\text{NO}_3^-)$   
48 can be considered as an indicator of anthropogenic combustion (Elliott et al., 2009; Fang et al., 2011), although this  
49 judgment may be influenced by isotopic exchange between NO and NO<sub>2</sub> (Freyer et al., 1993; Walters et al., 2016), **isotopic**  
50 **fractionations associated with nitrate formation pathways and isotopic effects occurring during transport, such as deposition**  
51 **of NO<sub>3</sub><sup>-</sup> and HNO<sub>3</sub> partitioning between gas and particle phase (Freyer, 1991; Geng et al., 2014).** The oxygen-17 excess  
52 ( $\Delta^{17}\text{O}$ ) of nitrate, defined as  $\Delta^{17}\text{O} = \delta^{17}\text{O} - 0.52\delta^{18}\text{O}$ , wherein  $\delta^{\text{X}}\text{O} = (R_{\text{sample}}/R_{\text{reference}} - 1)$  with  $R$  representing isotope ratios  
53 of  $^{\text{X}}\text{O}/^{16}\text{O}$  in the sample and the reference Vienna Standard Mean Ocean Water and X = 17 or 18, is particularly useful in  
54 reflecting nitrate formation pathways (Michalski et al., 2003). Atmospheric nitrate from nocturnal reaction pathways has  
55 higher  $\Delta^{17}\text{O}$  than that from daytime OH oxidation at given  $\Delta^{17}\text{O}(\text{NO}_2)$  (Table 1). **And once formed**, atmospheric  $\Delta^{17}\text{O}(\text{NO}_3^-)$   
56 cannot be altered by mass-dependent processes such as deposition during transport (Brenninkmeijer et al., 2003). Previous  
57 studies have shown the utility of atmospheric  $\Delta^{17}\text{O}(\text{NO}_3^-)$  in quantifying the relative importance of various nitrate formation  
58 pathways (Alexander et al., 2009; Michalski et al., 2003; Patris et al., 2007; Savarino et al., 2013; Vicars et al., 2013). For  
59 example,  $\Delta^{17}\text{O}(\text{NO}_3^-)$ -constrained box modeling work of Michalski et al. (2003) suggests that more than 90 % of

60 atmospheric nitrate is from nocturnal  $\text{N}_2\text{O}_5 + \text{H}_2\text{O}$  pathway in winter La Jolla, California, which is reflected by the highest  
61  $\Delta^{17}\text{O}(\text{NO}_3^-)$  values being observed in winter. In another study, Alexander et al. (2009) use observed  $\Delta^{17}\text{O}(\text{NO}_3^-)$  to constrain  
62 3D model and found that daytime  $\text{NO}_2 + \text{OH}$  pathway dominates global tropospheric nitrate production with an annual mean  
63 contribution of 76 %.

64 Until now, however, field observations of atmospheric  $\Delta^{17}\text{O}(\text{NO}_3^-)$  have not been conducted in north China to constrain  
65 the relative importance of different nitrate formation pathways during haze. In this work, we present the first observations of  
66 atmospheric  $\Delta^{17}\text{O}(\text{NO}_3^-)$  during Beijing haze from October 2014 to January 2015, and use this observation to examine the  
67 importance of nocturnal formation pathways. We also present the signature of simultaneously observed  $\delta^{15}\text{N}(\text{NO}_3^-)$ .

## 68 **2 Materials and Methods**

### 69 **2.1 Sampling and atmospheric observations**

70  $\text{PM}_{2.5}$  filter samples were collected at a flow rate of  $1.05 \text{ m}^3 \text{ min}^{-1}$  by a high volume air sampler (model TH-1000C II,  
71 Tianhong Instruments Co., Ltd, China). The filter is quartz microfiber filter (Whatman Inc., UK), pre-combusted at  $450^\circ\text{C}$   
72 for 4 h before sampling. Our sampling period lasted from October 2014 to January 2015 with the collection interval being 12  
73 h (08:00 – 20:00 LT or 20:00 – 08:00 LT) for each sample. Blank control samples were also collected. The blank was  
74 sampled identically to the real sample except that the collection interval is 1 min. Due to that gaseous  $\text{HNO}_3$  is likely to  
75 adsorb onto particulate matter already trapped by the filter material (Vicars et al., 2013), the nitrate species collected is likely  
76 to include both particulate nitrate and gaseous  $\text{HNO}_3$ , which is referred to as atmospheric nitrate in previous studies (Vicars  
77 et al., 2013; Morin et al., 2009; Michalski et al., 2003) and in this study. The **sampling site** is at the campus of University of  
78 the Chinese Academy of Sciences ( $40.41^\circ\text{N}$ ,  $116.68^\circ\text{E}$ , ~20 m high) in suburban Beijing, about 60 km northeast of  
79 downtown (Fig. 2), which is **a super site set by HOPE-J<sup>3</sup>A** (Haze Observation Project Especially for Jing-Jin-Ji Area) with  
80 various observations being reported (Zhang et al., 2017; Xu et al., 2016; Chen et al., 2015; Tong et al., 2015; He et al., 2018).  
81 Hourly concentrations of surface  $\text{PM}_{2.5}$ ,  $\text{CO}$ ,  $\text{SO}_2$ ,  $\text{NO}_2$  and  $\text{O}_3$  were observed at Huairou station ( $40.33^\circ\text{N}$ ,  $116.63^\circ\text{E}$ ) by  
82 Beijing Municipal Environmental Monitoring Center, **about 10 km to our sampling site**. Meteorological data including  
83 relative humidity (RH) and air temperature ( $T$ ) were measured by an automatic weather station (model MetPak, Gill  
84 Instruments Limited, UK). Time used in the present study is local time (LT = UTC + 8).

### 85 **2.2 Measurements of ions and isotopic ratios**

86 Ion concentrations of  $\text{NO}_3^-$  and  $\text{Cl}^-$  were measured in Anhui Province Key Laboratory of Polar Environment and Global

87 Change in the University of Science and Technology of China. A detailed description of this method can be found in the  
 88 literature (Ye et al., 2015). Briefly, ions in the PM<sub>2.5</sub> filter sample were extracted with Millipore water ( $\geq 18 \text{ M}\Omega$ ) and  
 89 insoluble substances in the extract were filtered. Then the ion concentrations were analyzed by an ion chromatograph system  
 90 (model Dionex ICS-2100, Thermo Fisher Scientific Inc., USA). The measured ion concentrations of blank samples were  
 91 subtracted when determining the ion concentrations of real samples. Typical analytical precision by our method is better than  
 92 10 % relative standard deviation (RSD) (Chen et al., 2016).

93  $\delta^{15}\text{N}(\text{NO}_3^-)$  and  $\Delta^{17}\text{O}(\text{NO}_3^-)$  were measured with a bacterial denitrifier method (Kaiser et al., 2007) in IsoLab at the  
 94 University of Washington, USA. Briefly, ions in the filter sample were extracted with Millipore water ( $\geq 18 \text{ M}\Omega$ ) and the  
 95 insoluble substances were filtered.  $\text{NO}_3^-$  in each sample was converted to  $\text{N}_2\text{O}$  by the denitrifying bacteria, *Pseudomonas*  
 96 *aureofaciens*. Then  $\text{N}_2$  and  $\text{O}_2$ , which were decomposed from  $\text{N}_2\text{O}$  in a gold tube at  $800^\circ \text{C}$ , were separated by a gas  
 97 chromatograph. The isotopic ratios of each gas were then measured by a Finnigan Delta-Plus Advantage isotope ratio mass  
 98 spectrometer. Masses of 28 and 29 from  $\text{N}_2$  were measured to determine  $\delta^{15}\text{N}$ . Masses of 32, 33 and 34 from  $\text{O}_2$  were  
 99 measured to determine  $\delta^{17}\text{O}$  and  $\delta^{18}\text{O}$  and  $\Delta^{17}\text{O}$  was then calculated. We use international nitrate reference materials,  
 100 USGS34, USGS35 and IAEANO<sub>3</sub>, for data calibration. The uncertainty ( $1\sigma$ ) of  $\delta^{15}\text{N}$  and  $\Delta^{17}\text{O}$  measurements in our method  
 101 is 0.4 ‰ and 0.2 ‰, respectively, based on replicate analysis of the international reference materials. All the samples  
 102 including blank samples were measured in triplicate to quantify the uncertainty in each sample. The blank was subtracted for  
 103 each sample by using an isotopic mass balance on the basis of isotopic ratios and concentrations of the blank. To minimize  
 104 the blank effect, samples with blank concentrations being  $> 10\%$  of their concentrations were not analyzed for isotopic  
 105 ratios. This ruled out 3 of the total 34 samples, all of which are in non-polluted days (NPD,  $\text{PM}_{2.5} < 75 \mu\text{g m}^{-3}$ ). Totally,  
 106 isotopic compositions of 7 samples in NPD and 24 samples in polluted days (PD,  $\text{PM}_{2.5} \geq 75 \mu\text{g m}^{-3}$ ) are reported here.

### 107 2.3 Estimate of different nitrate formation pathways based on $\Delta^{17}\text{O}(\text{NO}_3^-)$

108 The observed  $\Delta^{17}\text{O}(\text{NO}_3^-)$  is determined by the relative importance of different nitrate formation pathways and the  
 109 relative importance of  $\text{O}_3$  oxidation in  $\text{NO}_x$  cycling as shown in Eq. (1):

$$110 \Delta^{17}\text{O}(\text{NO}_3^-) = \Delta^{17}\text{O}_{\text{R6}} \times f_{\text{R6}} + \Delta^{17}\text{O}_{\text{R7}} \times f_{\text{R7}} + \Delta^{17}\text{O}_{\text{R8}} \times f_{\text{R8}} + \Delta^{17}\text{O}_{\text{R9}} \times f_{\text{R9}} + \Delta^{17}\text{O}_{\text{R10}} \times f_{\text{R10}} \quad (1)$$

111 Where  $\Delta^{17}\text{O}_{\text{R6}}$ ,  $\Delta^{17}\text{O}_{\text{R7}}$ ,  $\Delta^{17}\text{O}_{\text{R8}}$ ,  $\Delta^{17}\text{O}_{\text{R9}}$  and  $\Delta^{17}\text{O}_{\text{R10}}$  is respectively  $\Delta^{17}\text{O}(\text{NO}_3^-)$  resulting from  $\text{NO}_2 + \text{OH}$ ,  $\text{NO}_2 + \text{H}_2\text{O}$ ,  $\text{NO}_3 +$   
 112  $\text{HC}$ ,  $\text{N}_2\text{O}_5 + \text{H}_2\text{O}$  and  $\text{N}_2\text{O}_5 + \text{Cl}^-$  pathway (Table 1).  $f_{\text{R6}}$ ,  $f_{\text{R7}}$ ,  $f_{\text{R8}}$ ,  $f_{\text{R9}}$  and  $f_{\text{R10}}$  is respectively corresponding fractional  
 113 contribution of above pathways to nitrate production. By using the  $\Delta^{17}\text{O}$  assumptions for different pathways in Table 1 and  
 114 the definition  $f_{\text{R6}} + f_{\text{R7}} + f_{\text{R8}} + f_{\text{R9}} + f_{\text{R10}} = 1$ , Eq. (1) is further expressed as:

$$115 \Delta^{17}\text{O}(\text{NO}_3^-)/\text{‰} = 25\alpha f_{\text{R6}} + 25\alpha f_{\text{R7}} + (25\alpha + 14) \times f_{\text{R8}} + (25\alpha + 7) \times f_{\text{R9}} + (25\alpha + 14) \times f_{\text{R10}} = 25\alpha + 14 \times$$

$$116 (f_{\text{R8}} + f_{\text{R10}}) + 7f_{\text{R9}} \quad (2)$$

117 Where  $\alpha$  is the proportion of O<sub>3</sub> oxidation in NO<sub>2</sub> production rate, calculated by Eq. (3):

$$118 \quad \alpha = \frac{k_{R1}[NO][O_3]}{k_{R1}[NO][O_3] + k_{R2a}[NO][HO_2] + k_{R2b}[NO][RO_2]} \quad (3)$$

119 In Eq. (3),  $k_{R1}$ ,  $k_{R2a}$  and  $k_{R2b}$  is respectively the reaction rate constant listed in Table 2. To evaluate  $\alpha$ , we estimated HO<sub>2</sub>  
120 mixing ratios on the basis of empirical formulas between HO<sub>2</sub> and O<sub>3</sub> mixing ratios derived from observations in winter  
121 (Kanaya et al., 2007), that's:  $[HO_2]/(\text{pmol mol}^{-1}) = \exp(5.7747 \times 10^{-2} \times [O_3]/(\text{nmol mol}^{-1}) - 1.7227)$  during the day time and  
122  $[HO_2]/(\text{pmol mol}^{-1}) = \exp(7.7234 \times 10^{-2} \times [O_3]/(\text{nmol mol}^{-1}) - 1.6363)$  at night. Then RO<sub>2</sub> mixing ratio was calculated as 70 %  
123 of HO<sub>2</sub> mixing ratios based on previous studies (Liu et al., 2012; Elshorbany et al., 2012; Mihelcic et al., 2003). As NO  
124 mixing ratio was not observed in our study, we estimated NO mixing ratios following the empirical formulas between NO<sub>x</sub>  
125 and CO mixing ratios derived from observations in winter Beijing (Lin et al., 2011), that's:  $[NO]/(\text{nmol mol}^{-1}) =$   
126  $([CO]/(\text{nmol mol}^{-1}) - 196)/27.3 - [NO_2]/(\text{nmol mol}^{-1})$  during daytime and  $[NO]/(\text{nmol mol}^{-1}) = ([CO]/(\text{nmol mol}^{-1}) -$   
127  $105)/30.9 - [NO_2]/(\text{nmol mol}^{-1})$  at night.

128 By using Eq. (2), the relative importance of nocturnal formation pathways ( $f_{R8} + f_{R9} + f_{R10}$ ) can be written as Eq. (4):

$$129 \quad f_{R8} + f_{R9} + f_{R10} = \frac{f_{R9}}{2} + \frac{\Delta^{17}O(\text{NO}_3^-)}{14\text{‰}} - 1.8\alpha \quad (4)$$

130 Eq. (4) suggests that the relative importance of nocturnal pathways is solely a function of the assumption of  $f_{R9}$  at given  
131  $\Delta^{17}O(\text{NO}_3^-)$  and  $\alpha$ . Since  $f_{R9}$ ,  $f_{R8} + f_{R10}$  and  $f_{R8} + f_{R9} + f_{R10}$  should be in the range of 0 – 1 **all the time**,  $f_{R9}$  is further limited to  
132 meet Eq. (5):

$$133 \quad f_{R9} \begin{cases} > 0 \\ < \min(1, \frac{\Delta^{17}O(\text{NO}_3^-)}{7\text{‰}} - 3.6\alpha, 2 + 3.6\alpha - \frac{\Delta^{17}O(\text{NO}_3^-)}{7\text{‰}}) \end{cases} \quad (5)$$

134 We estimated the relative importance of nocturnal pathways ( $f_{R8} + f_{R9} + f_{R10}$ ) by using concentration-weighted  
135  $\Delta^{17}O(\text{NO}_3^-)$  observations and production rate weighted  $\alpha$  in PD of each haze event rather than each sample due to the  
136 lifetime of atmospheric nitrate is typically on the order of day (Liang et al., 1998), larger than our sampling collection  
137 interval.

## 138 2.4 Simulation of surface N<sub>2</sub>O<sub>5</sub> and NO<sub>3</sub> radical

139 **To see whether the relative importance of nocturnal pathways constrained by  $\Delta^{17}O(\text{NO}_3^-)$  can be reproduced by models,**  
140 we use the standard Master Chemical Mechanism (MCM, version 3.3, <http://mcm.leeds.ac.uk/>) to simulate the mixing  
141 ratios of surface N<sub>2</sub>O<sub>5</sub> and NO<sub>3</sub> radical during our sampling period. The input for this modeling work includes: (i) 1  
142 h-averaged mixing ratios of observed surface CO, NO<sub>2</sub>, SO<sub>2</sub> and O<sub>3</sub> and estimated NO (see Sect. 2.3), (ii) observed RH and  
143  $T$ , and (iii) the mixing ratios of organic compounds from the literatures (Table S1) (Wang et al., 2001; Wu et al., 2016; Rao et  
144 al., 2016).

## 146 3.1 Overview of observations in Beijing haze

147 Figure 3 describes general characteristics of haze events during our observations. The 12h-averaged  $PM_{2.5}$   
 148 concentrations, corresponding with filter samples, varied from 16 to 323  $\mu\text{g m}^{-3}$  with a mean of  $(141 \pm 88 \text{ (1SD)}) \mu\text{g m}^{-3}$ . In  
 149 comparison, the Grade II of NAAQS (National Ambient Air Quality Standard) in China is 75  $\mu\text{g m}^{-3}$  for daily  $PM_{2.5}$ . The  
 150  $NO_3^-$  concentrations present similar trends with  $PM_{2.5}$  levels (Fig. 3a), ranged from 0.3 to 106.7  $\mu\text{g m}^{-3}$  with a mean of  
 151  $(6.1 \pm 5.3) \mu\text{g m}^{-3}$  in non-polluted days (NPD,  $PM_{2.5} < 75 \mu\text{g m}^{-3}$ ) and  $(48.4 \pm 24.7) \mu\text{g m}^{-3}$  in polluted days (PD,  $PM_{2.5} \geq 75 \mu\text{g}$   
 152  $\text{m}^{-3}$ ). Correspondingly, the nitrogen oxidation ratio (NOR, which equals to  $NO_3^-$  molar concentration divided by the sum of  
 153  $NO_3^-$  and  $NO_2$  molar concentration), a proxy for secondary transformation of nitrate (Sun et al., 2006), increased from a  
 154 mean of  $0.09 \pm 0.05$  in NPD to  $0.31 \pm 0.10$  in PD (Fig. 3b). In residential heating season (Case III – V in November 2014 –  
 155 January 2015, Fig. 3b),  $Cl^-$  concentrations present similar trends with  $NO_3^-$  levels, increased from  $(0.6 \pm 1.0) \mu\text{g m}^{-3}$  in NPD  
 156 to  $(7.9 \pm 4.8) \mu\text{g m}^{-3}$  in PD. However, during Case I – II in October 2014,  $Cl^-$  concentrations were  $(3.5 \pm 1.6) \mu\text{g m}^{-3}$  in NPD  
 157 and  $(3.5 \pm 1.9) \mu\text{g m}^{-3}$  in PD, showing no significant difference at 0.01 level (t-test). Throughout our observational period, the  
 158 visibility decreased from  $(11.4 \pm 6.7) \text{ km}$  in NPD to  $(3.1 \pm 1.8) \text{ km}$  in PD (Fig. 3c) while relative humidity (RH) increased from  
 159  $(37 \pm 12) \%$  in NPD to  $(62 \pm 12) \%$  in PD (Fig. 3d).

160  $\Delta^{17}O(NO_3^-)$  ranged from 27.5 ‰ to 33.9 ‰ with the mean of  $(29.1 \pm 1.3) \%$  in NPD and  $(31.0 \pm 1.7) \%$  in PD (Fig. 3c).  
 161 Our observed  $\Delta^{17}O(NO_3^-)$  is in the range of  $\Delta^{17}O(NO_3^-)$  reported in literatures (Table 3) but at the high end of values from  
 162 other non-polar regions (Table 3). All our observed  $\Delta^{17}O(NO_3^-)$  values, no matter daytime sample (08:00 – 20:00) or  
 163 nighttime sample (20:00 – 08:00), are larger than 25 ‰, the maximum of  $\Delta^{17}O(NO_3^-)$  that can be produced via  $NO_2 + OH$   
 164 and  $NO_2 + H_2O$  (Table 1) at the assumption of bulk  $\Delta^{17}O(O_3) = 26 \%$  (Ishino et al., 2017; Vicars and Savarino, 2014). This  
 165 directly suggests nocturnal formation pathways ( $N_2O_5 + H_2O/Cl^-$  and  $NO_3 + HC$ ) must contribute to all the sampled nitrate.  
 166 Given the lifetime of atmospheric nitrate is typically larger than our sampling collection interval (Vicars et al., 2013), **each of**  
 167 **our samples** is expected to reflect both daytime and nocturnal nitrate production. Not surprisingly,  $\Delta^{17}O(NO_3^-)$  mean of  
 168 daytime and nighttime samples is  $(30.3 \pm 1.5) \%$  and  $(30.9 \pm 2.1) \%$ , respectively, showing no significant difference at 0.01  
 169 level (t-test).

170  $\delta^{15}N(NO_3^-)$  in our observation varied from  $-2.5 \%$  to 19.2 ‰ with a mean of  $(7.4 \pm 6.8) \%$ , which is in the range of  
 171  $\delta^{15}N(NO_3^-)$  observed from rainwater in Beijing, China (Zhang et al., 2008) and similar to  $\delta^{15}N(NO_3^-)$  values observed from  
 172 aerosols in Germany (Freyer, 1991). Figure 3d shows that  $\delta^{15}N(NO_3^-)$  varies largely in October 2014. The mean  $\delta^{15}N(NO_3^-)$   
 173 varied from  $(0.4 \pm 1.5) \%$  in 08:00 Oct. 18 – 08:00 Oct. 21 to  $(10.7 \pm 1.4) \%$  in 08:00 Oct. 21 – 08:00 Oct. 23 and then

174 decreased to  $(-0.9 \pm 2.1)$  ‰ in 08:00 Oct. 23 – 08:00 Oct. 26, which corresponds to  $PM_{2.5}$  concentrations being  $155 \pm 63$ ,  
175  $57 \pm 19$  and  $(188 \pm 51)$   $\mu\text{g m}^{-3}$  respectively. However, during residential heating season, relatively high  $\delta^{15}\text{N}(\text{NO}_3^-)$  ( $7.6 -$   
176  $19.2$  ‰) were always observed both in NPD and PD. This may be related to the high  $\text{NO}_x$  emission from coal combustion in  
177 north China (Wang et al., 2012; Lin, 2012; Zhang et al., 2007).

### 178 3.2 Relationships between $\Delta^{17}\text{O}(\text{NO}_3^-)$ and other data

179 Figure 4 presents the relationships between  $\Delta^{17}\text{O}(\text{NO}_3^-)$  and  $\text{NO}_3^-$  concentrations,  $PM_{2.5}$  concentrations, NOR, visibility,  
180 RH and  $\delta^{15}\text{N}(\text{NO}_3^-)$ .  $\Delta^{17}\text{O}(\text{NO}_3^-)$  shows a positive correlation with  $\text{NO}_3^-$  concentrations when  $\text{NO}_3^- < 50$   $\mu\text{g m}^{-3}$  ( $r = 0.81$ ,  $p$   
181  $< 0.01$ ). Similarly,  $\Delta^{17}\text{O}(\text{NO}_3^-)$  shows a positive correlation with  $PM_{2.5}$  concentration in Fig. 4b and NOR in Fig. 4c when  
182  $\text{NO}_3^- < 50$   $\mu\text{g m}^{-3}$  ( $r = 0.71$  and  $r = 0.80$ ,  $p < 0.01$ , respectively). Figure 4d shows that  $\Delta^{17}\text{O}(\text{NO}_3^-)$  is negative correlated with  
183 visibility in general ( $r = -0.66$ ,  $p < 0.01$ ). The significant decrease of visibility will largely reduce surface radiation and  
184 thereby OH mixing ratios (Zheng et al., 2015b), which is unfavorable for nitrate production via  $\text{NO}_2 + \text{OH}$  pathway. Since  
185  $\text{NO}_2 + \text{OH}$  pathway produces low  $\Delta^{17}\text{O}(\text{NO}_3^-)$  (Table 1), the decreased importance of  $\text{NO}_2 + \text{OH}$  pathway will conversely  
186 increase  $\Delta^{17}\text{O}(\text{NO}_3^-)$ . While the raise of RH accompanying the large increase of  $PM_{2.5}$  favors nitrate production via  
187 heterogeneous uptake of gases, e.g.,  $\text{N}_2\text{O}_5$  (Zheng et al., 2015b; Zheng et al., 2015a) and heterogeneous uptake of  $\text{N}_2\text{O}_5$   
188 produces relative high  $\Delta^{17}\text{O}(\text{NO}_3^-)$  (Table 1), the enhanced heterogeneous uptake of  $\text{N}_2\text{O}_5$  will increase  $\Delta^{17}\text{O}(\text{NO}_3^-)$  too.  
189 Therefore, the decrease of importance of  $\text{NO}_2 + \text{OH}$  and the increase of importance of heterogeneous uptake of  $\text{N}_2\text{O}_5$  should  
190 be responsible for the positive correlation between  $\Delta^{17}\text{O}(\text{NO}_3^-)$  and  $\text{NO}_3^-$  concentrations. In addition, for samples with  $\text{NO}_3^- >$   
191  $50$   $\mu\text{g m}^{-3}$ , visibility was always low with narrow variations ( $2.3 \pm 1.0$  km) and RH was always high with narrow range  
192 ( $67 \pm 7$  ‰), which may be responsible for the relatively high  $\Delta^{17}\text{O}(\text{NO}_3^-)$  being observed ( $31.2 \pm 1.7$  ‰). Figure 4f shows that  
193  $\Delta^{17}\text{O}(\text{NO}_3^-)$  is not correlated with  $\delta^{15}\text{N}(\text{NO}_3^-)$ .

### 194 3.3 Estimate of nocturnal formation pathways

195 Before estimating the relative importance of different nitrate formation pathways, we estimate the proportion of  $\text{O}_3$   
196 oxidation in  $\text{NO}_2$  production rate,  $\alpha$ . The possible  $\alpha$  range can be calculated based on observed  $\Delta^{17}\text{O}(\text{NO}_3^-)$ . It can be  
197 obtained from Table 1 that  $25\alpha$  ‰  $< \Delta^{17}\text{O}(\text{NO}_3^-) < (25\alpha + 14)$  ‰, so the lower limit of possible  $\alpha$  is  $(\Delta^{17}\text{O}(\text{NO}_3^-) -$   
198  $14$  ‰)/ $25$  ‰. And since  $\Delta^{17}\text{O}(\text{NO}_3^-) \geq 27.5$  ‰ in our observation, the higher limit of  $\alpha$  is always 1 for all the samples. Figure  
199 5 presents the possible range of calculated  $\alpha$  based on  $\Delta^{17}\text{O}(\text{NO}_3^-)$ . The calculated lower limit of  $\alpha$  ranged from 0.56 to 0.81  
200 with a mean of  $0.68 \pm 0.07$ , which directly suggests that  $\text{O}_3$  oxidation played a dominated role in  $\text{NO}_x$  cycling during Beijing  
201 haze. To estimate the specific  $\alpha$  value, chemical kinetics in Table 2 and Eq. (3) were used. Specific  $\alpha$  is estimated to range  
202 from 0.86 to 0.97 with a mean of  $(0.94 \pm 0.03)$ , which is in the possible range of  $\alpha$  value calculated directly based on

203  $\Delta^{17}\text{O}(\text{NO}_3^-)$  (Fig. 5) and close to the range of 0.85 – 1 determined in other mid-latitude areas (Michalski et al., 2003; Patris et  
204 al., 2007).

205 Figure 6a shows the estimated relative importance of nocturnal formation pathways ( $\text{N}_2\text{O}_5 + \text{H}_2\text{O}/\text{Cl}^-$  and  $\text{NO}_3 + \text{HC}$ )  
206 during PD of each case on the basis of observed  $\Delta^{17}\text{O}(\text{NO}_3^-)$ . Possible fractional contribution of nocturnal formation  
207 pathways ranges from 49 – 97 %, 58 – 100 %, 60 – 100 %, 45 – 90 % and 70 – 100 % in PD of Case I to V, respectively,  
208 with a mean of 56 – 97 %. This directly implies that nocturnal chemistry dominates atmospheric nitrate production in Beijing  
209 haze. This finding is consistent with the suggested importance of heterogeneous uptake of  $\text{N}_2\text{O}_5$  during Beijing haze by  
210 previous studies (Su et al., 2017; Wang et al., 2017b). The other pathways ( $\text{NO}_2 + \text{OH}$  and  $\text{NO}_2 + \text{H}_2\text{O}$ ) account for the  
211 remaining fraction with a mean possible range of 3 – 44 %. Since  $\text{NO}_2 + \text{OH}$  and  $\text{NO}_2 + \text{H}_2\text{O}$  produces the same  $\Delta^{17}\text{O}(\text{NO}_3^-)$   
212 signature in our assumptions (Table 1), we cannot distinguish their fractional contribution barely from the observed  
213  $\Delta^{17}\text{O}(\text{NO}_3^-)$  in the present study. However, the overall positive correlation between  $\Delta^{17}\text{O}(\text{NO}_3^-)$  and RH ( $r = 0.55$ ,  $p < 0.01$ ,  
214 Fig. 4e) suggests heterogeneous uptake of  $\text{NO}_2$  should be less important than heterogeneous uptake of  $\text{N}_2\text{O}_5$ , otherwise, a  
215 negative relationship between  $\Delta^{17}\text{O}(\text{NO}_3^-)$  and RH is expected. Our calculations also suggest that the sum of possible  
216 fractional contribution of  $\text{N}_2\text{O}_5 + \text{Cl}^-$  and  $\text{NO}_3 + \text{HC}$  is in the range of 0 – 49 %, 17 – 58 %, 20 – 60 %, 0 – 45 % and 41 – 70 %  
217 in PD of Case I to V, respectively, with a mean of 16 – 56 % (Table 4), which emphasizes that  $\text{N}_2\text{O}_5 + \text{Cl}^-$  and  $\text{NO}_3 + \text{HC}$   
218 played a non-ignorable role in nitrate production during Beijing haze. Due to that  $\text{N}_2\text{O}_5 + \text{Cl}^-$  and  $\text{NO}_3 + \text{HC}$  produce the  
219 same  $\Delta^{17}\text{O}(\text{NO}_3^-)$  in our assumptions (Table 1), we cannot distinguish their fractional contribution barely from the observed  
220  $\Delta^{17}\text{O}(\text{NO}_3^-)$  in this study, either. However,  $\text{NO}_3 + \text{HC}$  should be minor for nitrate production. For example, 3D modelling  
221 work of Alexander et al. (2009) suggests  $\text{NO}_3 + \text{HC}$  pathway only accounts for 4 % of global tropospheric nitrate production  
222 annually on average, and Michalski et al. (2003) found that  $\text{NO}_3 + \text{HC}$  pathway contributes 1 – 10 % to nitrate production on  
223 the basis of an annual observation at La Jolla, California, with low values in winter. Therefore, in addition to  $\text{NO}_3 + \text{HC}$ ,  
224  $\text{N}_2\text{O}_5 + \text{Cl}^-$  is likely to also contribute to nitrate production during haze in Beijing. Supportively, the concentrations of  $\text{Cl}^-$  is  
225 as high as  $(5.5 \pm 4.1) \mu\text{g m}^{-3}$  during PD of all the cases in our observation and the mixing ratios of  $\text{ClNO}_2$ , an indicator of  
226  $\text{N}_2\text{O}_5 + \text{Cl}^-$  pathway, reached up to  $2.9 \text{ nmol mol}^{-1}$  during a summer observation in suburban Beijing (Wang et al., 2018b)  
227 and reached up to  $5.0 \text{ nmol mol}^{-1}$  in a modelling work in summer rural Beijing (Wang et al., 2017c).

228 Figure 6b presents the simulated mixing ratios of surface  $\text{N}_2\text{O}_5$  and  $\text{NO}_3$  radical during our observational period by  
229 using the box model MCM. The 12h averaged mixing ratios of simulated  $\text{N}_2\text{O}_5$  ranged from 3 to  $649 \text{ pmol mol}^{-1}$  while  
230 simulated  $\text{NO}_3$  radical ranged from 0 to  $27 \text{ pmol mol}^{-1}$ . In comparison, previous observations in Beijing suggest 5s averaged  
231  $\text{N}_2\text{O}_5$  can be as high as  $1.3 \text{ nmol mol}^{-1}$  and 30 min averaged  $\text{NO}_3$  radical can be as high as  $38 \text{ pmol mol}^{-1}$  with large  
232 day-to-day variability (Wang et al., 2017b; Wang et al., 2015). During Case I and II in October, simulated  $\text{N}_2\text{O}_5$  and  $\text{NO}_3$   
233 radical present similar trends with the observed  $\text{NO}_3^-$  and remain relatively high during PD ( $346 \pm 128 \text{ pmol mol}^{-1}$  and  $9 \pm 7$



234 pmol mol<sup>-1</sup>, respectively, Fig. 6b), which supports the dominant role of nocturnal formation pathways suggested by  
235  $\Delta^{17}\text{O}(\text{NO}_3^-)$ . However, during Case III – V in residential heating season, the simulated surface mixing ratios of N<sub>2</sub>O<sub>5</sub> and  
236 NO<sub>3</sub> radical remain relatively low during PD (63±80 pmol mol<sup>-1</sup> and < 1 pmol mol<sup>-1</sup>, respectively, Fig. 6b), which seems to  
237 be inconsistent with  $\Delta^{17}\text{O}(\text{NO}_3^-)$  observations. We note that a recent study suggests that heterogeneous uptake of N<sub>2</sub>O<sub>5</sub> is  
238 negligible at surface but larger at higher altitudes (e.g., > 150 m) during winter haze in Beijing (Wang et al., 2018a). So  
239 during PD of Case III – V in our observational period, large nitrate production via heterogeneous uptake of N<sub>2</sub>O<sub>5</sub> may occur  
240 aloft rather than at surface, which leads to the dominant role of nocturnal formation pathways as suggested by  $\Delta^{17}\text{O}(\text{NO}_3^-)$ .

## 241 4 Conclusions

242 We report the first observation of isotopic composition ( $\Delta^{17}\text{O}$  and  $\delta^{15}\text{N}$ ) of atmospheric nitrate in Beijing haze. The  
243 observed  $\Delta^{17}\text{O}(\text{NO}_3^-)$  ranged from 27.5 ‰ to 33.9 ‰ with a mean of (30.6±1.8) ‰.  $\delta^{15}\text{N}(\text{NO}_3^-)$  ranged largely from -2.5 ‰  
244 to 19.2 ‰ with a mean of (7.4±6.8) ‰. When NO<sub>3</sub><sup>-</sup> is < 50 μg m<sup>-3</sup>, a positive correlation was observed between  $\Delta^{17}\text{O}(\text{NO}_3^-)$   
245 and NO<sub>3</sub><sup>-</sup> concentration (r = 0.81, p < 0.01). This is likely to result from the variation of relative importance of different  
246 nitrate formation pathway. **Calculations with the constraint of  $\Delta^{17}\text{O}(\text{NO}_3^-)$  suggest that nocturnal pathways (N<sub>2</sub>O<sub>5</sub> + H<sub>2</sub>O/Cl<sup>-</sup>  
247 and NO<sub>3</sub> + HC) dominated nitrate production during polluted days (PM<sub>2.5</sub> ≥ 75 μg m<sup>-3</sup>), with the mean possible contribution  
248 of 56 – 97 %.  $\Delta^{17}\text{O}(\text{NO}_3^-)$  also indicates that O<sub>3</sub> dominated NO oxidation during Beijing haze.**

## 249 Supplementary Materials

250 **Figure S1.** The diurnal differences of observed NO<sub>2</sub>, CO and O<sub>3</sub> and calculated NO, HO<sub>2</sub> and RO<sub>2</sub> during our sampling  
251 periods.

252 **Table S1.** The input of organic compounds for MCM model (nmol mol<sup>-1</sup>).

## 253 Data availability

254 All data needed to draw the conclusions are present in the main text and/or the Supplementary Materials. For additional  
255 data, please contact the corresponding author (zqxie@ustc.edu.cn).

256 **Author contributions**

257 Z.Q.X. conceived this study. P.Z.H. conducted isotope measurements. P.Z.H., X.Y.C, S.D.F, H.C.Z., H. K. performed  
258 the field experiments and ion measurements. P.Z.H., Z.Q.X., X.W.Y. interpreted the data. C.L. contributed to the field  
259 observation support. P.Z.H. wrote the manuscript with Z.Q.X. inputs. All authors involved the discussion and revision.

260 **Competing interests**

261 The authors declare no competing interests.

262 **Acknowledgments**

263 This work was supported by the National Key Project of MOST (2016YFC0203302), NSFC (91544013), the Key  
264 Project of CAS (KJZD-EW-TZ-G06-01) and the Atmospheric Pollution Control of the Prime Minister (DQGG0104). We  
265 gratefully thank staffs of IsoLab at UW for their technical support, Becky Alexander and Lei Geng for helpful discussions.

266 **References**

- 267 Alexander, B., Hastings, M. G., Allman, D. J., Dachs, J., Thornton, J. A., and Kunasek, S. A.: Quantifying atmospheric  
268 nitrate formation pathways based on a global model of the oxygen isotopic composition ( $\Delta^{17}\text{O}$ ) of atmospheric nitrate,  
269 *Atmos. Chem. Phys.*, 9, 5043-5056, 2009.
- 270 Berhanu, T. A., Savarino, J., Bhattacharya, S. K., and Vicars, W. C.:  $^{17}\text{O}$  excess transfer during the  $\text{NO}_2 + \text{O}_3 \rightarrow \text{NO}_3 + \text{O}_2$   
271 reaction, *J. Chem. Phys.*, 136, 044311, 2012.
- 272 Bertram, T. H., and Thornton, J. A.: Toward a general parameterization of  $\text{N}_2\text{O}_5$  reactivity on aqueous particles: the  
273 competing effects of particle liquid water, nitrate and chloride, *Atmos. Chem. Phys.*, 9, 8351-8363, 2009.
- 274 Beyn, F., Matthias, V., and Dänke, K.: Changes in atmospheric nitrate deposition in Germany—An isotopic perspective,  
275 *Environ. Pollut.*, 194, 1-10, 2014.
- 276 Brenninkmeijer, C. A., Janssen, C., Kaiser, J., Röckmann, T., Rhee, T. S., and Assonov, S. S.: Isotope effects in the chemistry  
277 of atmospheric trace compounds, *Chem. Rev.*, 103, 5125-5162, 2003.
- 278 Brook, R. D., Rajagopalan, S., Pope, C. A., Brook, J. R., Bhatnagar, A., Diez-Roux, A. V., Holguin, F., Hong, Y., Luepker, R.  
279 V., and Mittleman, M. A.: Particulate matter air pollution and cardiovascular disease an update to the scientific

280 statement from the American Heart Association, *Circulation*, 121, 2331-2378, 2010.

281 Brown, S. S., and Stutz, J.: Nighttime radical observations and chemistry, *Chem. Soc. Rev.*, 41, 6405-6447, 2012.

282 Burkholder, J. B., Sander, S. P., Abbatt, J. P. D., Barker, J. R., Huie, R. E., Kolb, C. E., Kurylo, M. J., Orkin, V. L., Wilmouth,  
283 D. M., and Wine, P. H.: *Chemical Kinetics and Photochemical Data for Use in Atmospheric Studies: Evaluation*  
284 *Number 18*, Pasadena, CA: Jet Propulsion Laboratory, National Aeronautics and Space Administration, 2015.

285 Chen, Q., Geng, L., Schmidt, J. A., Xie, Z., Kang, H., Dachs, J., Cole-Dai, J., Schauer, A. J., Camp, M. G., and Alexander, B.:  
286 Isotopic constraints on the role of hypohalous acids in sulfate aerosol formation in the remote marine boundary layer,  
287 *Atmos. Chem. Phys.*, 16, 11433-11450, 2016.

288 Chen, Z., Zhang, J., Zhang, T., Liu, W., and Liu, J.: Haze observations by simultaneous lidar and WPS in Beijing before and  
289 during APEC, 2014, *Sci. China Chem.*, 58, 1385-1392, 2015.

290 Cheng, Z., Jiang, J., Fajardo, O., Wang, S., and Hao, J.: Characteristics and health impacts of particulate matter pollution in  
291 China (2001–2011), *Atmos. Environ.*, 65, 186-194, 2013.

292 Cheung, J. L., Li, Y., Boniface, J., Shi, Q., Davidovits, P., Worsnop, D. R., Jayne, J. T., and Kolb, C. E.: Heterogeneous  
293 interactions of NO<sub>2</sub> with aqueous surfaces, *J. Phys. Chem. A*, 104, 2655-2662, 2000.

294 Elliott, E. M., Kendall, C., Boyer, E. W., Burns, D. A., Lear, G. G., Golden, H. E., Harlin, K., Bytnerowicz, A., Butler, T. J.,  
295 and Glatz, R.: Dual nitrate isotopes in dry deposition: Utility for partitioning NO<sub>x</sub> source contributions to landscape  
296 nitrogen deposition, *J. Geophys. Res. Biogeo.*, 114, 2009.

297 Elshorbany, Y. F., Kleffmann, J., Hofzumahaus, A., Kurtenbach, R., Wiesen, P., Brauers, T., Bohn, B., Dorn, H. P., Fuchs, H.,  
298 and Holland, F.: HO<sub>x</sub> budgets during HO<sub>x</sub>Comp: A case study of HO<sub>x</sub> chemistry under NO<sub>x</sub> - limited conditions, *J.*  
299 *Geophys. Res.*, 117, 2012.

300 Fang, Y., Koba, K., Wang, X., Wen, D., Li, J., Takebayashi, Y., Liu, X., and Yoh, M.: Anthropogenic imprints on nitrogen and  
301 oxygen isotopic composition of precipitation nitrate in a nitrogen-polluted city in southern China, *Atmos. Chem. Phys.*,  
302 11, 1313-1325, 2011.

303 Felix, J. D., Elliott, E. M., and Shaw, S. L.: Nitrogen isotopic composition of coal-fired power plant NO<sub>x</sub>: influence of  
304 emission controls and implications for global emission inventories, *Environ. Sci. Technol.*, 46, 3528-3535, 2012.

305 Freyer, H. D.: Seasonal variation of <sup>15</sup>N/<sup>14</sup>N ratios in atmospheric nitrate species, *Tellus B*, 43, 30-44, 1991.

306 Freyer, H. D., Kley, D., Volz - Thomas, A., and Kobel, K.: On the interaction of isotopic exchange processes with  
307 photochemical reactions in atmospheric oxides of nitrogen, *J. Geophys. Res. Atmos.*, 98, 14791-14796, 1993.

308 Geng, L., Alexander, B., Cole-Dai, J., Steig, E. J., Savarino, J., Sofen, E. D., and Schauer, A. J.: Nitrogen isotopes in ice core  
309 nitrate linked to anthropogenic atmospheric acidity change, *Proc. Natl. Acad. Sci. USA*, 111, 5808-5812, 2014.

310 Goodman, A. L., Underwood, G. M., and Grassian, V. H.: Heterogeneous reaction of NO<sub>2</sub>: Characterization of gas-phase

311 and adsorbed products from the reaction,  $2\text{NO}_2(\text{g}) + \text{H}_2\text{O}(\text{a}) \rightarrow \text{HONO}(\text{g}) + \text{HNO}_3(\text{a})$  on hydrated silica particles, *J.*  
312 *Phys. Chem. A*, 103, 7217-7223, 1999.

313 Guha, T., Lin, C. T., Bhattacharya, S. K., Mahajan, A. S., Ou-Yang, C.-F., Lan, Y.-P., Hsu, S. C., and Liang, M.-C.: Isotopic  
314 ratios of nitrate in aerosol samples from Mt. Lulin, a high-altitude station in Central Taiwan, *Atmos. Environ.*, 154,  
315 53-69, 2017.

316 Hastings, M. G., Casciotti, K. L., and Elliott, E. M.: Stable isotopes as tracers of anthropogenic nitrogen sources, deposition,  
317 and impacts, *Elements*, 9, 339-344, 2013.

318 He, P., Alexander, B., Geng, L., Chi, X., Fan, S., Zhan, H., Kang, H., Zheng, G., Cheng, Y., Su, H., Liu, C., and Xie, Z.:  
319 Isotopic constraints on heterogeneous sulfate production in Beijing haze, *Atmos. Chem. Phys.*, 18, 5515-5528, 2018.

320 Hoering, T.: The isotopic composition of the ammonia and the nitrate ion in rain, *Geochim. Cosmochim. Acta*, 12, 97-102,  
321 1957.

322 Ishino, S., Hattori, S., Savarino, J., Jourdain, B., Preunkert, S., Legrand, M., Caillon, N., Barbero, A., Kuribayashi, K., and  
323 Yoshida, N.: Seasonal variations of triple oxygen isotopic compositions of atmospheric sulfate, nitrate, and ozone at  
324 Dumont d'Urville, coastal Antarctica, *Atmos. Chem. Phys.*, 17, 3713-3727, 2017.

325 Kaiser, J., Hastings, M. G., Houlton, B. Z., Röckmann, T., and Sigman, D. M.: Triple oxygen isotope analysis of nitrate using  
326 the denitrifier method and thermal decomposition of  $\text{N}_2\text{O}$ , *Anal. Chem.*, 79, 599-607, 2007.

327 Kanaya, Y., Cao, R., Akimoto, H., Fukuda, M., Komazaki, Y., Yokouchi, Y., Koike, M., Tanimoto, H., Takegawa, N., and  
328 Kondo, Y.: Urban photochemistry in central Tokyo: 1. Observed and modeled OH and HO<sub>2</sub> radical concentrations  
329 during the winter and summer of 2004, *J. Geophys. Res.*, 112, 2007.

330 Kunasek, S. A., Alexander, B., Steig, E. J., Hastings, M. G., Gleason, D. J., and Jarvis, J. C.: Measurements and modeling of  
331  $\Delta^{17}\text{O}$  of nitrate in snowpits from Summit, Greenland, *J. Geophys. Res.*, 113, 2008.

332 Li, H., Zhu, T., Zhao, D., Zhang, Z., and Chen, Z.: Kinetics and mechanisms of heterogeneous reaction of  $\text{NO}_2$  on  $\text{CaCO}_3$   
333 surfaces under dry and wet conditions, *Atmos. Chem. Phys.*, 10, 463-474, 2010.

334 Li, Z., Hu, R., Xie, P., Wang, H., Lu, K., and Wang, D.: Intercomparison of in situ CRDS and CEAS for measurements of  
335 atmospheric  $\text{N}_2\text{O}_5$  in Beijing, China, *Sci. Total Environ.*, 613, 131-139, 2018.

336 Liang, J., Horowitz, L. W., Jacob, D. J., Wang, Y., Fiore, A. M., Logan, J. A., Gardner, G. M., and Munger, J. W.: Seasonal  
337 budgets of reactive nitrogen species and ozone over the United States, and export fluxes to the global atmosphere, *J.*  
338 *Geophys. Res. Atmos.*, 103, 13435-13450, 1998.

339 Lin, J.-T.: Satellite constraint for emissions of nitrogen oxides from anthropogenic, lightning and soil sources over East  
340 China on a high-resolution grid, *Atmos. Chem. Phys.*, 12, 2881-2898, 2012.

341 Lin, W., Xu, X., Ge, B., and Liu, X.: Gaseous pollutants in Beijing urban area during the heating period 2007–2008:

342 variability, sources, meteorological, and chemical impacts, *Atmos. Chem. Phys.*, 11, 8157-8170, 2011.

343 Liu, Z., Wang, Y., Gu, D., Zhao, C., Huey, L., Stickel, R., Liao, J., Shao, M., Zhu, T., and Zeng, L.: Summertime  
344 photochemistry during CAREBeijing-2007: ROx budgets and O<sub>3</sub> formation, *Atmos. Chem. Phys.*, 12, 7737-7752, 2012.

345 Michalski, G., Scott, Z., Kabling, M., and Thiemens, M. H.: First measurements and modeling of  $\Delta^{17}\text{O}$  in atmospheric  
346 nitrate, *Geophys. Res. Lett.*, 30, 2003.

347 Mihelcic, D., Holland, F., Hofzumahaus, A., Hoppe, L., Konrad, S., M $\ddot{u}$ sgen, P., P $\ddot{a}$ tz, H. W., Sch $\ddot{a}$ fer, H. J., Schmitz, T., and  
348 Volz - Thomas, A.: Peroxy radicals during BERLIOZ at Pabstthum: Measurements, radical budgets and ozone  
349 production, *J. Geophys. Res.*, 108, 2003.

350 Morin, S., Savarino, J., Bekki, S., Cavender, A., Shepson, P. B., and Bottenheim, J. W.: Major influence of BrO on the NOx  
351 and nitrate budgets in the Arctic spring, inferred from  $\Delta^{17}\text{O}(\text{NO}_3^-)$  measurements during ozone depletion events,  
352 *Environ. Chem.*, 4, 238, 2007a.

353 Morin, S., Savarino, J., Bekki, S., Gong, S., and Bottenheim, J. W.: Signature of Arctic surface ozone depletion events in the  
354 isotope anomaly ( $\Delta^{17}\text{O}$ ) of atmospheric nitrate, *Atmos. Chem. Phys.*, 7, 1451-1469, 2007b.

355 Morin, S., Savarino, J., Frey, M. M., Yan, N., Bekki, S., Bottenheim, J. W., and Martins, J. M.: Tracing the origin and fate of  
356 NOx in the Arctic atmosphere using stable isotopes in nitrate, *Science*, 322, 730-732, 2008.

357 Morin, S., Savarino, J., Frey, M. M., Domine, F., Jacobi, H. W., Kaleschke, L., and Martins, J. M.: Comprehensive isotopic  
358 composition of atmospheric nitrate in the Atlantic Ocean boundary layer from 65 S to 79 N, *J. Geophys. Res. Atmos.*,  
359 114, 2009.

360 Morin, S., Sander, R., and Savarino, J.: Simulation of the diurnal variations of the oxygen isotope anomaly ( $\Delta^{17}\text{O}$ ) of reactive  
361 atmospheric species, *Atmos. Chem. Phys.*, 11, 3653-3671, 2011.

362 Pathak, R. K., Wu, W. S., and Wang, T.: Summertime PM<sub>2.5</sub> ionic species in four major cities of China: nitrate formation in  
363 an ammonia-deficient atmosphere, *Atmos. Chem. Phys.*, 9, 1711-1722, 2009.

364 Pathak, R. K., Wang, T., and Wu, W. S.: Nighttime enhancement of PM<sub>2.5</sub> nitrate in ammonia-poor atmospheric conditions  
365 in Beijing and Shanghai: plausible contributions of heterogeneous hydrolysis of N<sub>2</sub>O<sub>5</sub> and HNO<sub>3</sub> partitioning, *Atmos.*  
366 *Environ.*, 45, 1183-1191, 2011.

367 Patris, N., Cliff, S. S., Quinn, P. K., Kasem, M., and Thiemens, M. H.: Isotopic analysis of aerosol sulfate and nitrate during  
368 ITCT - 2k2: Determination of different formation pathways as a function of particle size, *J. Geophys. Res. Atmos.*, 112,  
369 2007.

370 Rao, Z., Chen, Z., Liang, H., Huang, L., and Huang, D.: Carbonyl compounds over urban Beijing: Concentrations on haze  
371 and non-haze days and effects on radical chemistry, *Atmos. Environ.*, 124, 207-216, 2016.

372 Savarino, J., and Thiemens, M. H.: Analytical procedure to determine both  $\delta^{18}\text{O}$  and  $\delta^{17}\text{O}$  of H<sub>2</sub>O<sub>2</sub> in natural water and first

373 measurements, *Atmos. Environ.*, 33, 3683-3690, 1999.

374 Savarino, J., Kaiser, J., Morin, S., Sigman, D. M., and Thiemens, M. H.: Nitrogen and oxygen isotopic constraints on the  
375 origin of atmospheric nitrate in coastal Antarctica, *Atmos. Chem. Phys.*, 7, 1925-1945, 2007.

376 Savarino, J., Bhattacharya, S. K., Morin, S., Baroni, M., and Doussin, J.-F.: The NO + O<sub>3</sub> reaction: A triple oxygen isotope  
377 perspective on the reaction dynamics and atmospheric implications for the transfer of the ozone isotope anomaly, *J.*  
378 *Chem. Phys.*, 128, 194303, 2008.

379 Savarino, J., Morin, S., Erbland, J., Grannec, F., Patey, M. D., Vicars, W., Alexander, B., and Achterberg, E. P.: Isotopic  
380 composition of atmospheric nitrate in a tropical marine boundary layer, *P. Natl. Acad. Sci. USA*, 110, 17668-17673,  
381 2013.

382 Sofen, E. D., Alexander, B., Steig, E. J., Thiemens, M. H., Kunasek, S. A., Amos, H. M., Schauer, A. J., Hastings, M. G.,  
383 Bautista, J., and Jackson, T. L.: WAIS Divide ice core suggests sustained changes in the atmospheric formation  
384 pathways of sulfate and nitrate since the 19th century in the extratropical Southern Hemisphere, *Atmos. Chem. Phys.*,  
385 14, 5749-5769, 2014.

386 Su, X., Tie, X., Li, G., Cao, J., Huang, R., Feng, T., Long, X., and Xu, R.: Effect of hydrolysis of N<sub>2</sub>O<sub>5</sub> on nitrate and  
387 ammonium formation in Beijing China: WRF-Chem model simulation, *Sci. Total Environ.*, 579, 221-229, 2017.

388 Sun, Y., Zhuang, G., Tang, A., Wang, Y., and An, Z.: Chemical characteristics of PM<sub>2.5</sub> and PM<sub>10</sub> in haze-fog episodes in  
389 Beijing, *Environ. Sci. Technol.*, 40, 3148-3155, 2006.

390 Tong, S., Hou, S., Zhang, Y., Chu, B., Liu, Y., He, H., Zhao, P., and Ge, M.: Comparisons of measured nitrous acid (HONO)  
391 concentrations in a pollution period at urban and suburban Beijing, in autumn of 2014, *Sci. China Chem.*, 58,  
392 1393-1402, 2015.

393 Vicars, W. C., Morin, S., Savarino, J., Wagner, N. L., Erbland, J., Vince, E., Martins, J. M. F., Lerner, B. M., Quinn, P. K.,  
394 and Coffman, D. J.: Spatial and diurnal variability in reactive nitrogen oxide chemistry as reflected in the isotopic  
395 composition of atmospheric nitrate: Results from the CalNex 2010 field study, *J. Geophys. Res. Atmos.*, 118, 2013.

396 Vicars, W. C., and Savarino, J.: Quantitative constraints on the 17O-excess ( $\Delta^{17}\text{O}$ ) signature of surface ozone: Ambient  
397 measurements from 50°N to 50°S using the nitrite-coated filter technique, *Geochim. Cosmochim. Acta*, 135, 270-287,  
398 2014.

399 Walters, W. W., Simonini, D. S., and Michalski, G.: Nitrogen isotope exchange between NO and NO<sub>2</sub> and its implications for  
400  $\delta^{15}\text{N}$  variations in tropospheric NO<sub>x</sub> and atmospheric nitrate, *Geophys. Res. Lett.*, 43, 440-448, 2016.

401 Wang, D., Hu, R., Xie, P., Liu, J., Liu, W., Qin, M., Ling, L., Zeng, Y., Chen, H., Xing, X., Zhu, G., Wu, J., Duan, J., Lu, X.,  
402 and Shen, L.: Diode laser cavity ring-down spectroscopy for in situ measurement of NO<sub>3</sub> radical in ambient air, *J. Quant.*  
403 *Spectrosc. Radiat. Transf.*, 166, 23-29, 2015.

404 Wang, H., Chen, J., and Lu, K.: Development of a portable cavity-enhanced absorption spectrometer for the measurement of  
405 ambient  $\text{NO}_3$  and  $\text{N}_2\text{O}_5$ : experimental setup, lab characterizations, and field applications in a polluted urban  
406 environment, *Atmos. Meas. Tech.*, 10, 1465, 2017a.

407 Wang, H., Lu, K., Chen, X., Zhu, Q., Chen, Q., Guo, S., Jiang, M., Li, X., Shang, D., and Tan, Z.: High  $\text{N}_2\text{O}_5$  concentrations  
408 observed in urban Beijing: Implications of a large nitrate formation pathway, *Environ. Sci. Technol. Lett.*, 4, 416-420,  
409 2017b.

410 Wang, H., Lu, K., Tan, Z., Sun, K., Li, X., Hu, M., Shao, M., Zeng, L., Zhu, T., and Zhang, Y.: Model simulation of  $\text{NO}_3$ ,  
411  $\text{N}_2\text{O}_5$  and  $\text{ClNO}_2$  at a rural site in Beijing during CAREBeijing-2006, *Atmos. Res.*, 196, 97-107, 2017c.

412 Wang, H., Lu, K., Chen, X., Zhu, Q., Wu, Z., Wu, Y., and Sun, K.: Large particulate nitrate formation from  $\text{N}_2\text{O}_5$  uptake in a  
413 chemically reactive layer aloft during wintertime in Beijing, *Atmos. Chem. Phys. Discuss.*, 1-27, 2018a.

414 Wang, H., Lu, K., Guo, S., Wu, Z., Shang, D., Tan, Z., Wang, Y., Le Breton, M., Zhu, W., Lou, S., Tang, M., Wu, Y., Zheng,  
415 J., Zeng, L., Hallquist, M., Hu, M., and Zhang, Y.: Efficient  $\text{N}_2\text{O}_5$  Uptake and  $\text{NO}_3$  Oxidation in the Outflow of Urban  
416 Beijing, *Atmos. Chem. Phys. Discuss.*, 1-27, 2018b.

417 Wang, J., Zhang, X., Guo, J., Wang, Z., and Zhang, M.: Observation of nitrous acid (HONO) in Beijing, China: Seasonal  
418 variation, nocturnal formation and daytime budget, *Sci. Total Environ.*, 587, 350-359, 2017d.

419 Wang, S., Zhang, Q., Streets, D. G., He, K., Martin, R. V., Lamsal, L. N., Chen, D., Lei, Y., and Lu, Z.: Growth in  $\text{NO}_x$   
420 emissions from power plants in China: bottom-up estimates and satellite observations, *Atmos. Chem. Phys.*, 12,  
421 4429-4447, 2012.

422 Wang, Y., Zhou, L., Wang, M., and Zheng, X.: Trends of atmospheric methane in Beijing, *Chemosphere*, 3, 65-71, 2001.

423 Wen, L., Chen, J., Yang, L., Wang, X., Xu, C., Sui, X., Yao, L., Zhu, Y., Zhang, J., and Zhu, T.: Enhanced formation of fine  
424 particulate nitrate at a rural site on the North China Plain in summer: The important roles of ammonia and ozone, *Atmos.*  
425 *Environ.*, 101, 294-302, 2015.

426 Wu, R., Li, J., Hao, Y., Li, Y., Zeng, L., and Xie, S.: Evolution process and sources of ambient volatile organic compounds  
427 during a severe haze event in Beijing, China, *Sci. Total Environ.*, 560, 62-72, 2016.

428 Xiao, H., Xie, L., Long, A., Ye, F., Pan, Y., Li, D., Long, Z., Chen, L., Xiao, H., and Liu, C.: Use of isotopic compositions of  
429 nitrate in TSP to identify sources and chemistry in South China Sea, *Atmos. Environ.*, 109, 70-78, 2015.

430 Xu, X., Zhao, W., Zhang, Q., Wang, S., Fang, B., Chen, W., Venables, D. S., Wang, X., Pu, W., and Wang, X.: Optical  
431 properties of atmospheric fine particles near Beijing during the HOPE-J3 A campaign, *Atmos. Chem. Phys.*, 16,  
432 6421-6439, 2016.

433 Ye, P., Xie, Z., Yu, J., and Kang, H.: Spatial distribution of methanesulphonic acid in the Arctic aerosol collected during the  
434 Chinese Arctic Research Expedition, *Atmosphere*, 6, 699-712, 2015.

435 Yu, Z., and Elliott, E. M.: Novel Method for Nitrogen Isotopic Analysis of Soil-Emitted Nitric Oxide, *Environ. Sci. Technol.*,  
 436 2017.

437 Zhang, J., Chen, Z., Lu, Y., Gui, H., Liu, J., Liu, W., Wang, J., Yu, T., Cheng, Y., and Chen, Y.: Characteristics of aerosol size  
 438 distribution and vertical backscattering coefficient profile during 2014 APEC in Beijing, *Atmos. Environ.*, 148, 30-41,  
 439 2017.

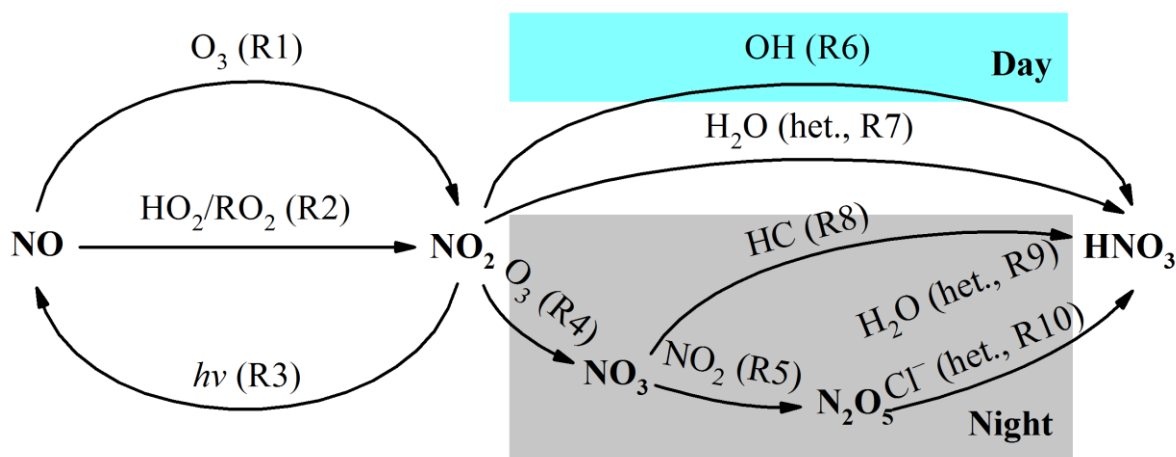
440 Zhang, Q., Streets, D. G., He, K., Wang, Y., Richter, A., Burrows, J. P., Uno, I., Jang, C. J., Chen, D., Yao, Z., and Lei, Y.:  
 441 NO<sub>x</sub> emission trends for China, 1995–2004: The view from the ground and the view from space, *J. Geophys. Res.*, 112,  
 442 2007.

443 Zhang, Y., Liu, X., Fangmeier, A., Goulding, K. T. W., and Zhang, F.: Nitrogen inputs and isotopes in precipitation in the  
 444 North China Plain, *Atmos. Environ.*, 42, 1436-1448, 2008.

445 Zheng, B., Zhang, Q., Zhang, Y., He, K., Wang, K., Zheng, G., Duan, F., Ma, Y., and Kimoto, T.: Heterogeneous chemistry: a  
 446 mechanism missing in current models to explain secondary inorganic aerosol formation during the January 2013 haze  
 447 episode in North China, *Atmos. Chem. Phys.*, 15, 2031-2049, 2015a.

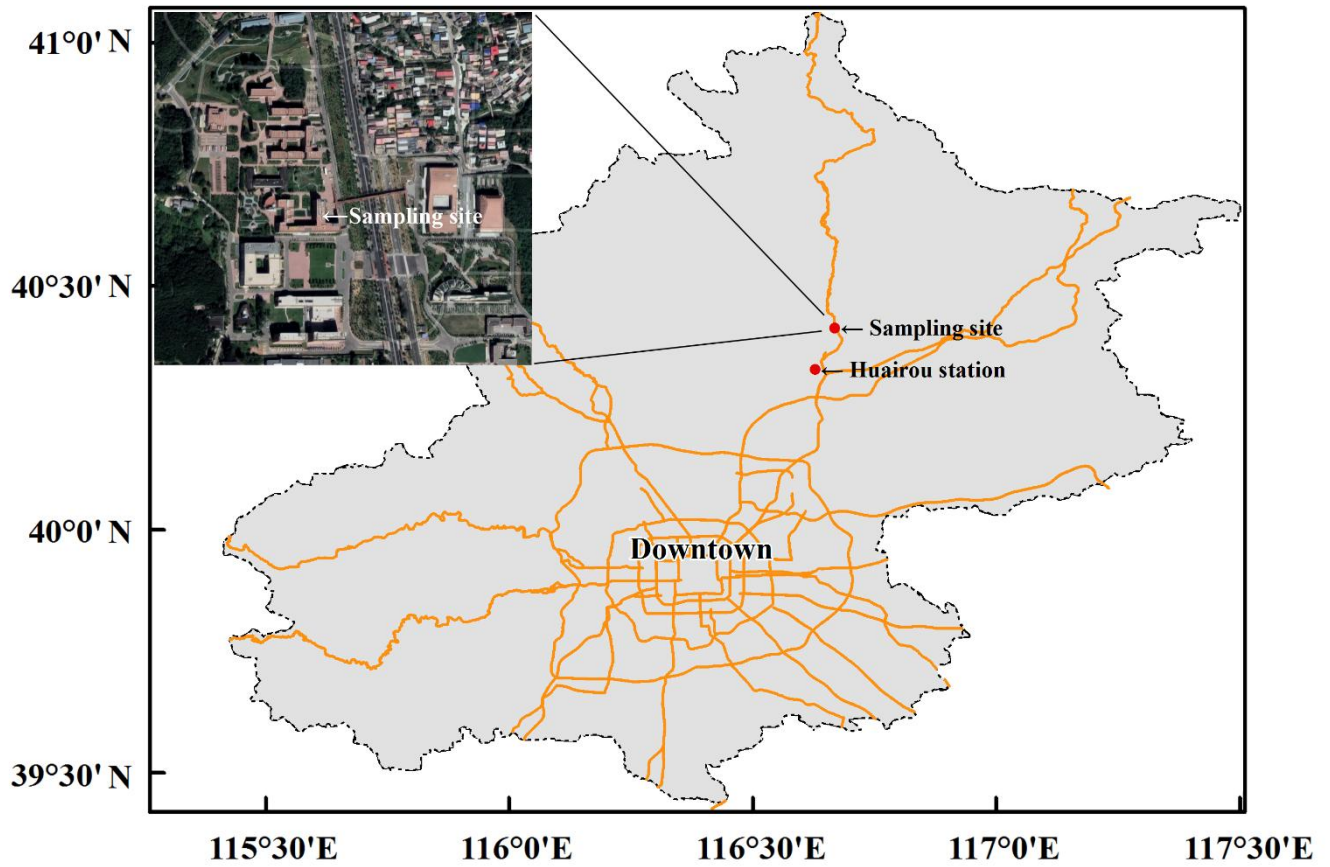
448 Zheng, G., Duan, F., Su, H., Ma, Y., Cheng, Y., Zheng, B., Zhang, Q., Huang, T., Kimoto, T., and Chang, D.: Exploring the  
 449 severe winter haze in Beijing: the impact of synoptic weather, regional transport and heterogeneous reactions, *Atmos.*  
 450 *Chem. Phys.*, 15, 2969-2983, 2015b.

451 **Figures and Tables**



452  
 453 **Figure 1.** Simplified schematic of the main nitrate formation pathways in urban air. “het.” means heterogeneous reactions on  
 454 aerosols.

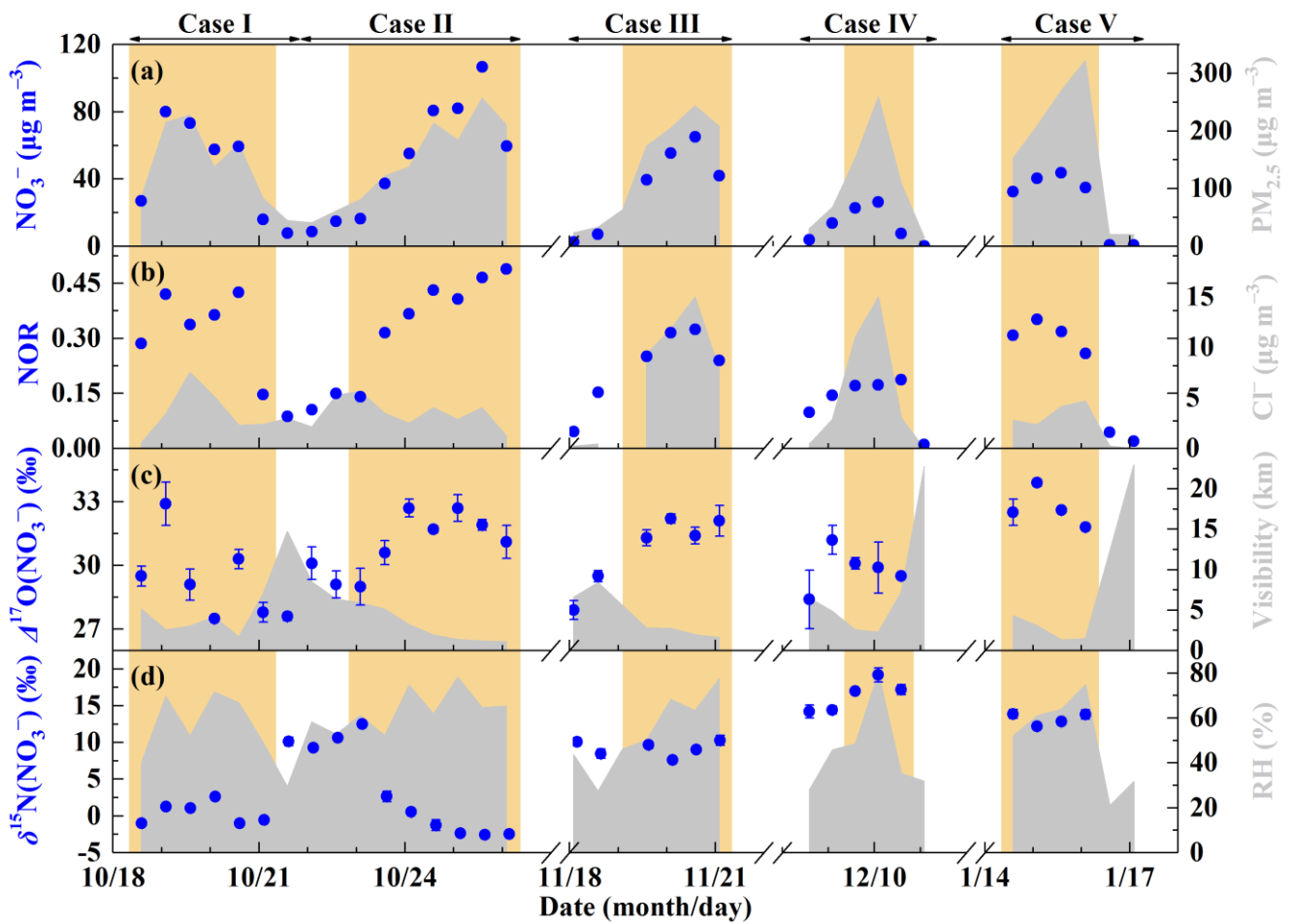




455

456 **Figure 2.** A brief map of sampling site in Beijing. The map scale of base map is 1:1250000. Huairou station is set by Beijing

457 Municipal Environmental Monitoring Center, where hourly  $PM_{2.5}$ ,  $SO_2$ , CO,  $NO_2$  and  $O_3$  were observed.



458

459

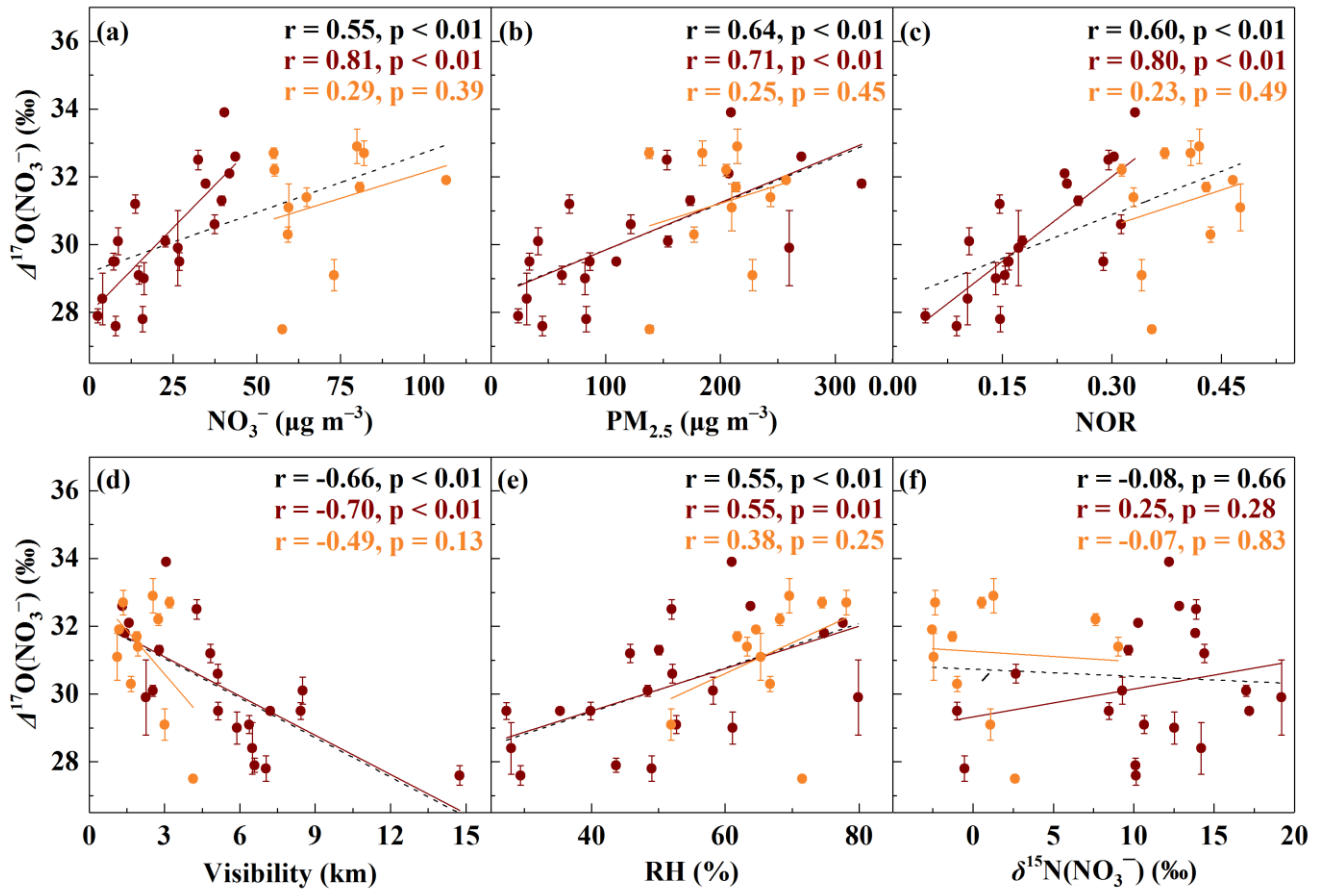
460

461

462

463

**Figure 3.** General characteristics of haze events in Beijing (October 2014 – January 2015). (a) Time series of  $\text{PM}_{2.5}$  and  $\text{NO}_3^-$  concentrations. (b) Time series of nitrogen oxidation ratio (NOR, which equals to  $\text{NO}_3^-$  molar concentration divided by the sum of  $\text{NO}_3^-$  and  $\text{NO}_2$  molar concentration) and  $\text{Cl}^-$  concentrations. (c) Time series of  $\Delta^{17}\text{O}(\text{NO}_3^-)$  and visibility. (d) Time series of  $\delta^{15}\text{N}(\text{NO}_3^-)$  and relative humidity (RH). The error bars in (c) and (d) are  $\pm 1\sigma$  of replicate measurements ( $n = 3$ ) of each sample. The khaki shaded area indicates polluted days (PD,  $\text{PM}_{2.5} \geq 75 \mu\text{g m}^{-3}$ ).



464

465

466

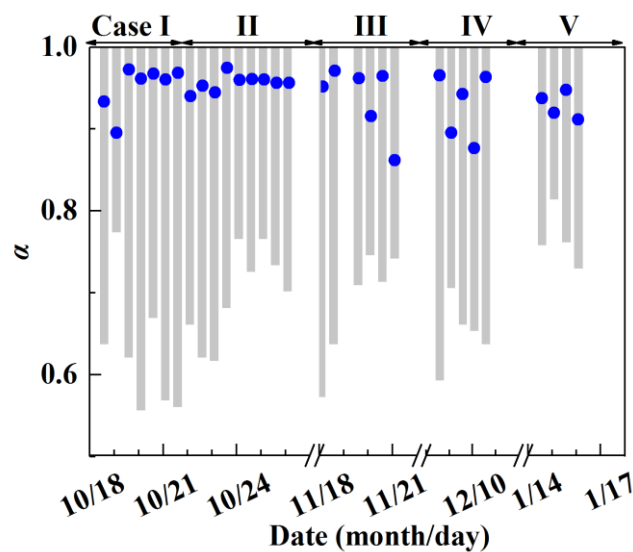
467

468

469

470

**Figure 4.** Relationships between  $\Delta^{17}\text{O}(\text{NO}_3^-)$  and other parameters. The relationship between  $\Delta^{17}\text{O}(\text{NO}_3^-)$  and  $\text{NO}_3^-$  concentrations (a),  $\text{PM}_{2.5}$  concentrations (b), nitrogen oxidation ratio (NOR, c), visibility (d), relative humidity (RH, e) and  $\delta^{15}\text{N}(\text{NO}_3^-)$  (f). The dark red dots are samples with  $\text{NO}_3^- < 50 \mu\text{g m}^{-3}$  and the orange dots are samples with  $\text{NO}_3^- > 50 \mu\text{g m}^{-3}$ . The black dash lines are linear least-squares fitting lines for all samples, the dark red solid lines are linear least-squares fitting lines for samples with  $\text{NO}_3^- < 50 \mu\text{g m}^{-3}$  and the orange solid lines are linear least-squares fitting lines for samples with  $\text{NO}_3^- > 50 \mu\text{g m}^{-3}$ . The error bars are  $\pm 1\sigma$  of replicate measurements of each sample.

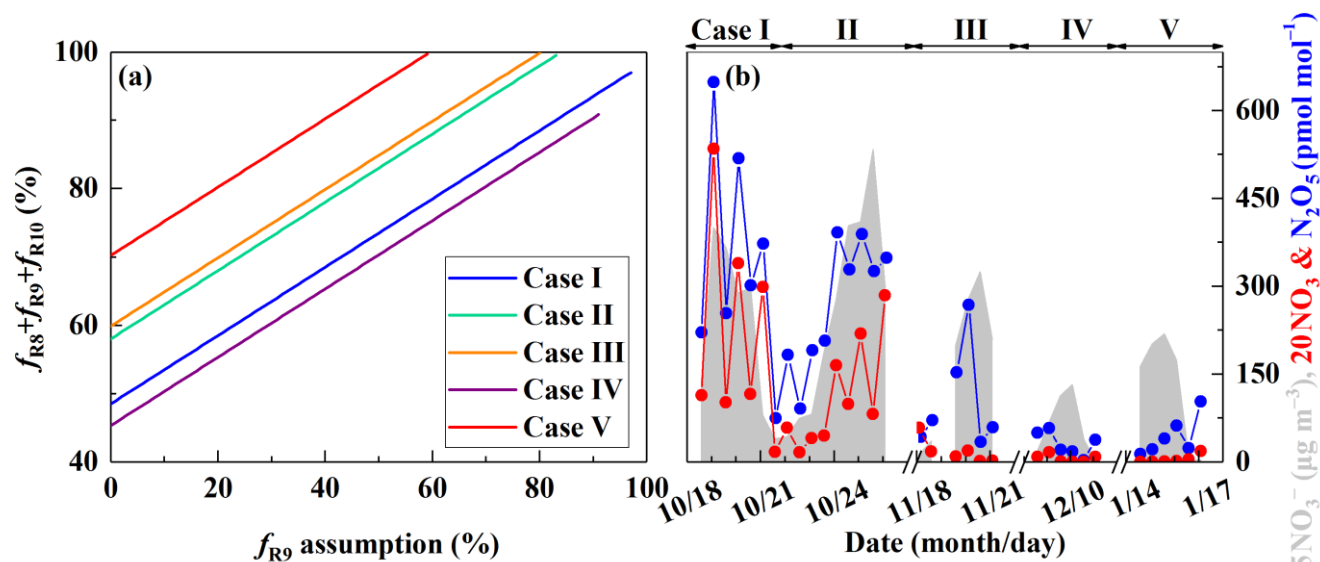


471

472

**Figure 5.** Estimate of the proportion of  $\text{O}_3$  oxidation in  $\text{NO}_x$  cycling,  $\alpha$ . The gray column represents possible  $\alpha$  range

473 determined by  $\Delta^{17}\text{O}(\text{NO}_3^-)$ . The blue dot represents specific  $\alpha$  value calculated by Eq. (3).



474  
 475 **Figure 6.** Estimate of the nocturnal formation pathways. The estimated relative importance of nocturnal formation pathways  
 476 ( $f_{R8} + f_{R9} + f_{R10}$ ) during PD of each case on the basis of observed  $\Delta^{17}\text{O}(\text{NO}_3^-)$  (See Sect. 2.3, a) and the simulated mixing  
 477 ratios of  $\text{N}_2\text{O}_5$  and  $\text{NO}_3$  radical by MCM (b). R8, R9 and R10 in (a) represents  $\text{NO}_3 + \text{HC}$ ,  $\text{N}_2\text{O}_5 + \text{H}_2\text{O}$  and  $\text{N}_2\text{O}_5 + \text{Cl}^-$   
 478 pathway, respectively.

479 **Table 1.** Isotope assumptions of different nitrate formation pathways.

No.	Reaction	$\Delta^{17}\text{O}$ of product		Reference
		Expression	Value (‰) <sup>a</sup>	
R1	$\text{NO} + \text{O}_3 \rightarrow \text{NO}_2 + \text{O}_2$	$\Delta^{17}\text{O}(\text{NO}_2) = 1.18 \times \Delta^{17}\text{O}(\text{O}_3) + 6.6 \text{‰}$	37	(Savarino et al., 2008)
R2	$\text{NO} + \text{HO}_2/\text{RO}_2 \rightarrow \text{NO}_2 + \text{OH}/\text{RO}$	$\Delta^{17}\text{O}(\text{NO}_2) = 0.0$	0.0	(Sofen et al., 2014)
R4	$\text{NO}_2 + \text{O}_3 \rightarrow \text{NO}_3 + \text{O}_2$	$\Delta^{17}\text{O}(\text{NO}_3) =$ $\frac{2}{3}\Delta^{17}\text{O}(\text{NO}_2) + \frac{1}{3}(1.23 \times \Delta^{17}\text{O}(\text{O}_3) + 9.0 \text{‰})$	$25\alpha + 14$	(Berhanu et al., 2012)
R5	$\text{NO}_2 + \text{NO}_3 \rightarrow \text{N}_2\text{O}_5$	$\Delta^{17}\text{O}(\text{N}_2\text{O}_5) = \frac{2}{5}\Delta^{17}\text{O}(\text{NO}_2) + \frac{3}{5}\Delta^{17}\text{O}(\text{NO}_3)$	$30\alpha + 8$	(Sofen et al., 2014)
R6	$\text{NO}_2 + \text{OH} \rightarrow \text{HNO}_3$	$\Delta^{17}\text{O}(\text{NO}_3^-) = \frac{2}{3}\Delta^{17}\text{O}(\text{NO}_2)$	$25\alpha$	(Sofen et al., 2014)
R7	$2\text{NO}_2 + \text{H}_2\text{O} \rightarrow \text{HNO}_3 + \text{HNO}_2$	$\Delta^{17}\text{O}(\text{NO}_3^-) = \frac{2}{3}\Delta^{17}\text{O}(\text{NO}_2)$	$25\alpha$	<sup>b</sup>
R8	$\text{NO}_3 + \text{HC} \rightarrow \text{HNO}_3 + \text{products}$	$\Delta^{17}\text{O}(\text{NO}_3^-) = \Delta^{17}\text{O}(\text{NO}_3)$	$25\alpha + 14$	(Sofen et al., 2014)
R9	$\text{N}_2\text{O}_5 + \text{H}_2\text{O} \rightarrow 2\text{HNO}_3$	$\Delta^{17}\text{O}(\text{NO}_3^-) = \frac{5}{6}\Delta^{17}\text{O}(\text{N}_2\text{O}_5)$	$25\alpha + 7$	(Sofen et al., 2014)
R10	$\text{N}_2\text{O}_5 + \text{Cl}^- \rightarrow \text{HNO}_3 + \text{ClNO}_2$	$\Delta^{17}\text{O}(\text{NO}_3^-) = \Delta^{17}\text{O}(\text{NO}_3)$	$25\alpha + 14$	<sup>c</sup>

480 <sup>a</sup> The values are calculated on assumptions that bulk  $\Delta^{17}\text{O}(\text{O}_3) = 26 \text{‰}$  (Vicars and Savarino, 2014; Ishino et al., 2017) and

481  $\Delta^{17}\text{O}(\text{HO}_2/\text{RO}_2) = 0 \text{‰}$ .  $\Delta^{17}\text{O}(\text{RO}_2)$  is equal to  $0 \text{‰}$  in the troposphere (Morin et al., 2011), in contrast, observations suggest

482  $\Delta^{17}\text{O}(\text{HO}_2) = 1 - 2 \text{ ‰}$  (Savarino and Thiemens, 1999). However, the difference in calculated  $\Delta^{17}\text{O}(\text{NO}_3^-)$  between assuming  
 483  $\Delta^{17}\text{O}(\text{HO}_2) = 0 \text{ ‰}$  and  $\Delta^{17}\text{O}(\text{HO}_2) = 2 \text{ ‰}$  is negligible in this study ( $< 0.1 \text{ ‰}$ ). And the assumption that  $\Delta^{17}\text{O}(\text{HO}_2) = 0 \text{ ‰}$   
 484 simplifies calculations and is also consistent with previous studies (Michalski et al., 2003; Alexander et al., 2009; Morin et  
 485 al., 2008; Kunasek et al., 2008; Sofen et al., 2014).  $\alpha$  is the proportion of  $\text{O}_3$  oxidation in  $\text{NO}_2$  production rate, calculated by  
 486 Eq. (3).

487 <sup>b</sup> Previous studies suggest that in R7 one oxygen atom of  $\text{NO}_3^-$  is from  $\text{H}_2\text{O}$  and the other two are from  $\text{NO}_2$  (Li et al., 2010;  
 488 Cheung et al., 2000; Goodman et al., 1999), which will result in  $\Delta^{17}\text{O}(\text{NO}_3^-) = 2/3\Delta^{17}\text{O}(\text{NO}_2)$ .

489 <sup>c</sup> R4 and R5 suggest that the central oxygen atom of  $\text{N}_2\text{O}_5$  ( $\text{O}_2\text{N-O-NO}_2$ ) is from  $\text{NO}_3$  radical ( $\text{O-NO}_2$ ) with  $\Delta^{17}\text{O} (\text{‰}) =$   
 490  $1.23 \times \Delta^{17}\text{O}(\text{O}_3) + 9.0 \text{ ‰}$ . R10 is suggested to occur via  $\text{O}_2\text{N-O-NO}_2 (\text{aq}) \leftrightarrow \text{NO}_2^+ + \text{NO}_3^-$  and the following  $\text{NO}_2^+ + \text{Cl}^- \rightarrow$   
 491  $\text{ClNO}_2$  (Bertram and Thornton, 2009), so  $\Delta^{17}\text{O}(\text{NO}_3^-) = 1/3(1.23 \times \Delta^{17}\text{O}(\text{O}_3) + 9.0 \text{ ‰}) + 2/3\Delta^{17}\text{O}(\text{NO}_2) = \Delta^{17}\text{O}(\text{NO}_3)$ .

492 **Table 2.** Reaction expressions for different  $\text{NO}_2$  production pathways.

No.	Reaction	Rate expression	Rate constant ( $\text{cm}^3 \text{ molecule}^{-1} \text{ s}^{-1}$ )	Reference
R1	$\text{NO} + \text{O}_3 \rightarrow \text{NO}_2 + \text{O}_2$	$k_{\text{R1}}[\text{NO}][\text{O}_3]$	$k_{\text{R1}} = 3.0 \times 10^{-12} \times e^{(-1500/T)}$	(Burkholder et al., 2015)
R2a	$\text{NO} + \text{HO}_2 \rightarrow \text{NO}_2 + \text{OH}$	$k_{2\text{Ra}}[\text{NO}][\text{HO}_2]$	$k_{2\text{Ra}} = 3.3 \times 10^{-12} \times e^{(270/T)}$	(Burkholder et al., 2015)
R2b	$\text{NO} + \text{RO}_2 \rightarrow \text{NO}_2 + \text{RO}$	$k_{2\text{Rb}}[\text{NO}][\text{RO}_2]$	$k_{2\text{Rb}} = k_{2\text{Ra}}$	(Burkholder et al., 2015; Kunasek et al., 2008)

493 **Table 3.** Atmospheric  $\Delta^{17}\text{O}(\text{NO}_3^-)$  in aerosols obtained from the literature and this study.

Sample location	Sample period	Collection interval	$\Delta^{17}\text{O} (\text{‰})$ range	Reference
Huairou, Beijing (40.41 °N, 116.68 °E)	October 2014 – January 2015	12 h	27.5 – 33.9 (30.6 ± 1.8)	This study
Trinidad Head, California (41.0 °N, 124.2 °W)	April – May 2002	1 – 4 days	20.1 – 27.5	(Patris et al., 2007)
La Jolla, California (32.7 °N, 117.2 °W)	March 1997 – April 1998	3 days	20 – 30.8	(Michalski et al., 2003)
Mt. Lulin, Taiwan (23.5 °N, 120.9 °E)	January – December 2010	1 day	2.7 – 31.4 (17 ± 7)	(Guha et al., 2017)
Cape Verde Island (16.9 °N, 24.9 °W)	July 2007 – May 2008	2 – 3 days	25.5 – 31.3	(Savarino et al., 2013)
Cruise in costal California (32.8 °N – 38.6 °N)	May – June 2010	2 – 22 h	19.0 – 29.2 (24.1 ± 2.2)	(Vicars et al., 2013)

Cruise from 65 °S to 79 °N	September – October 2006	1 – 4 days	Non-polar:	(Morin et al., 2009)
	April – May 2007		24 – 33	
	February – April 2006		Polar: 35 ± 2	
Alert, Nunavut (82.5 °N, 62.3 °W)	March – May 2004	3 – 4 days	29 – 35 (32.7 ± 1.8)	(Morin et al., 2007b)
Barrow, Alaska (71.3 °N, 156.9 °W)	March 2005	1 day	26 – 36	(Morin et al., 2007a)
Dumont d'Urville, Antarctic (66.7 °S, 140.0 °E)	January – December 2001	10 – 15 days	20.0 – 43.1	(Savarino et al., 2007)
Dumont d'Urville, Antarctic (66.7 °S, 140.0 °E)	January 2011 – January 2012	7 days	23.0 – 41.9	(Ishino et al., 2017)

494 **Table 4** The possible range of fractional contribution of different nitrate formation pathways during PD of each case  
 495 estimated on the basis of observed  $\Delta^{17}\text{O}(\text{NO}_3^-)$  <sup>a</sup>.

PD of Case	$f_{R9}$ assumption (%)	$f_{R8} + f_{R9} + f_{R10}$ (%)	$f_{R8} + f_{R10}$ (%)	$f_{R6} + f_{R7}$ (%)
I	0 – 97	49 – 97	0 – 49	3 – 51
II	0 – 83	58 – 100	17 – 58	0 – 42
III	0 – 80	60 – 100	20 – 60	0 – 40
IV	0 – 90	45 – 90	0 – 45	10 – 55
V	0 – 59	70 – 100	41 – 70	0 – 30
Average	0 – 82	56 – 97	16 – 56	3 – 44

496 <sup>a</sup> R6, R7, R8, R9 and R10 is respectively  $\text{NO}_2 + \text{OH}$ ,  $\text{NO}_2 + \text{H}_2\text{O}$ ,  $\text{NO}_3 + \text{HC}$ ,  $\text{N}_2\text{O}_5 + \text{H}_2\text{O}$  and  $\text{N}_2\text{O}_5 + \text{Cl}^-$  pathway.